Supplementary Information

Electrical characterization of a large-area single-layer Cu_3BHT 2D conjugated coordination polymer

Sandra. M. Estévez[a,b,#], Zhiyong Wang[d,e,#], Tsai-Jung Liu[e], Gabriel Caballero[a,c], Fernando J. Urbanos[a], Ignacio Figueruelo-Campanero[a,c], Julia García-Pérez[a], Cristina Navío[a], Miroslav Polozij[e,f,g], Jianjun Zhang[e], Thomas Heine[e,f,g,h], Mariela Menghini[a], Daniel Granados[a], Xiliang Feng[d,e,*], Renhao Dong[i,j,*], and Enrique Cánovas[a,*].

[a] *IMDEA Nanociencia, 28049 Madrid, Spain.*

[b] *Escuela de Doctorado, Universidad Autónoma de Madrid, 28049 Madrid, Spain.*

[c] *Facultad Ciencias Físicas, Universidad Complutense de Madrid, 28040 Madrid, Spain*

[d] *Max Planck Institute of Microstructure Physics, Halle (Saale), Germany.*

[e] *Center for Advancing Electronics Dresden (cfaed) & Faculty of Chemistry and Food Chemistry, Technische Universität Dresden, Germany.*

[f] *Helmholtz-Zentrum Dresden-Rossendorf (HZDR), Abteiling Ressoursenökilogie, 04318 Leipzig, Germany.*

[g] *Center for Advanced Systems Understanding, CASUS, Untermarkt 20, 02826 Görlitz, Germany.*

[h] *Department of Chemistry, Yonsei University, Seodaemun-gu, Seoul, 120-749 Republic of Korea*.

[i] *Key Laboratory of Colloid and Interface Chemistry of the Ministry of Education, School of Chemistry and Chemical Engineering, Shandong University, Jinan, 250199 China.*

[j] *Materials Innovation Institute for Life Sciences and Energy (MILES) & Department of Chemistry, University of Hong Kong, China.*

[#] These authors contributed equally

[*] Author to whom correspondence should be addressed: xinliang.feng@tu-dresden.de, renhaodong@sdu.edu.cn, enrique.canovas@imdea.org

- **Cu_3BHT characterization**

After the synthesis of Cu_3BHT, extensive characterization has been carried out to ensure that its properties are optimal for subsequent electrical measurements. Optical images (Figure S1), STEM-EDS mapping (Figure S2), SEM-EDX mapping (Figure S3), Raman spectra (Figure S4), and UV-Vis spectrum (Figure S5) have been obtained.

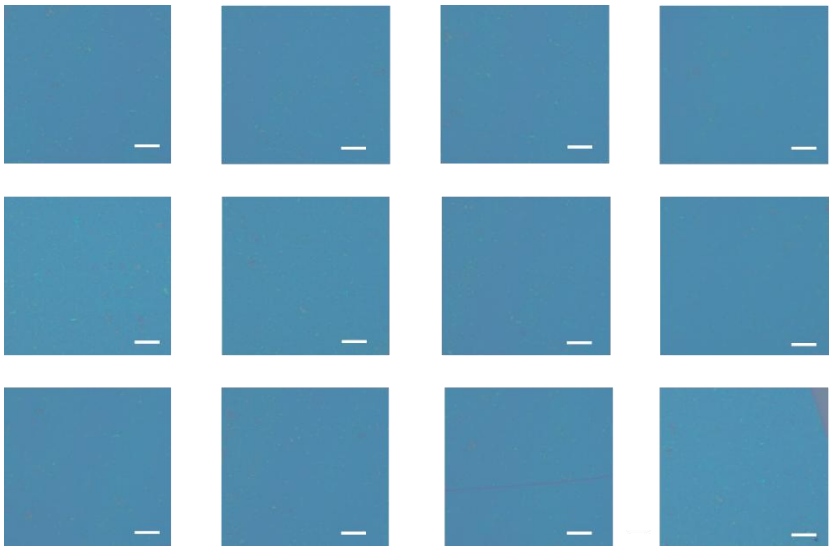

Figure S1. Optical microscopy images of single-layer Cu_3BHT on the SiO_2 substrate, captured across a cm^2-scale film (Scale bar, 10 μm). This result reveals a homogeneous nature of single-layer Cu_3BHT. Nevertheless, we acknowledge the presence of cracks and wrinkles at the edges, resulting from the transfer process.

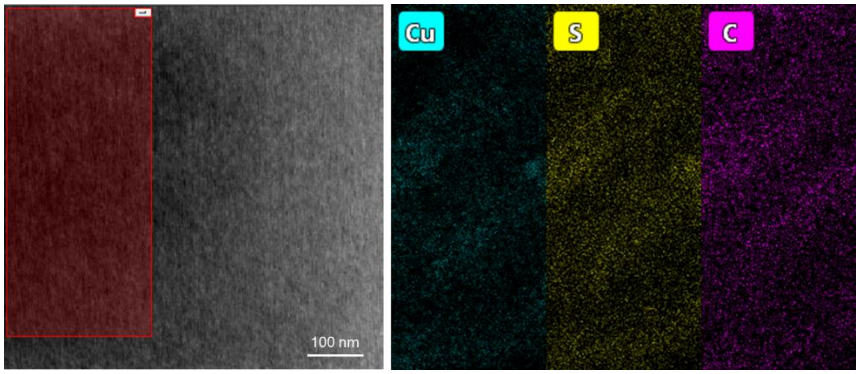

Figure S2. STEM-EDS mapping of Cu, S, and C elements across the single-layer Cu_3BHT.

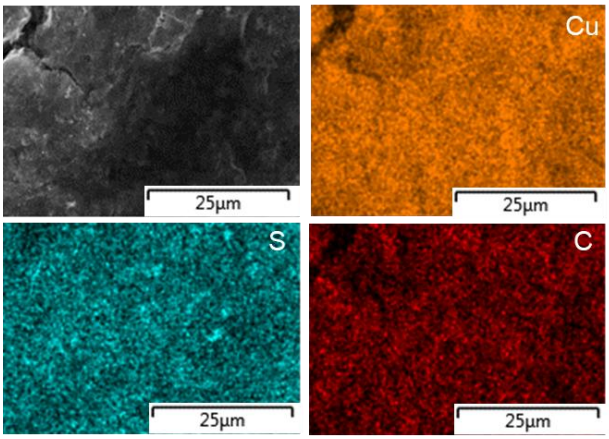

Figure S3. SEM-EDX mapping of Cu, S, and C elements across the 20-layer Cu_3BHT, prepared via layer-by-layer transfer to ensure sufficient signal and minimize background noise from the Si substrate.

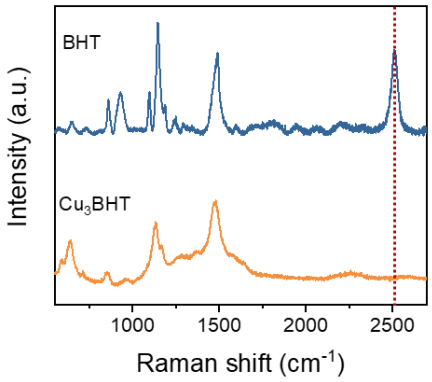

Figure S4. Surface-enhanced Raman spectra of BHT ligand and single-layer Cu_3BHT.

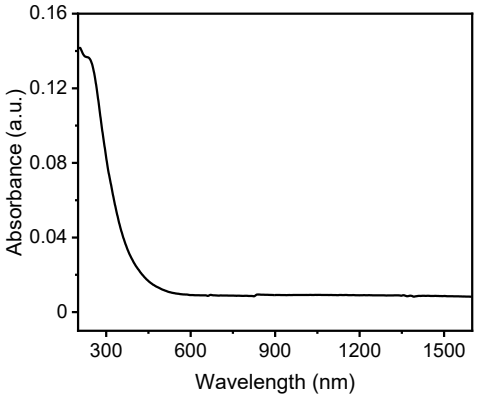

Figure S5. UV-Vis spectrum of single-layer Cu_3BHT.

- **Device fabrication**

For the fabrication of Cu_3BHT devices, commercial silicon substrates covered by 290 nm of thermally-grown silicon oxide layer were used. In all substrate, an arrangement of markers was defined in order to facilitate the location of devices later on. Different arrangement of electrodes, as depicted in Figure S6 were defined by UV maskless lithography process using AZ1505 positive resist. The metallic pads were fabricated by evaporation of 20/80 nm of Ti/Au followed by a lift-off in acetone at 50 ºC for 1 h. Three different types of devices were defined over the surface of SiO_2/Si substrate with 8×8 mm^2 area. The devices were distributed over 3 areas (C1-C4) as shown in Figure S6.a and Figure S10: 4 Van der Pauw devices (D1-D4); 2 Transfer Length Method (TLM) (D5) in areas C1 and C3; and 9 hall bridges (not used) in area C2. The C4 area was left blank for other characterizations. On the top left corner of each area (big electrode) a gate contact was defined by scratching the substrate to remove the SiO_2 in the area.

Two routes were followed to realize the Cu_3BHT devices:

- Route 1 – A layer of Cu_3BHT was transferred to the SiO_2/Si wafer with markers, then maskless UV lithography combined with reactive ion etching was used to define stripes of Cu_3BHT layer. After this, a second lithography step combined with evaporation was used to define metallic electrodes connected to the Cu_3BHT stripes. Although this route provides well-defined transport bridges ideal for electrical characterization, all prepared samples showed a highly insulating response (with R well above our detection limits). This behavior was likely due to the post-treatment of the monolayer Cu_3BHT. Further work is needed to ascertain the impact of the processing protocol on the sample electrical response.
- Route 2 – This fabrication method was designed to avoid any post-treatment of the monolayer Cu_3BHT, see Figure S7. This is achieved at the cost of having devices with a poorly defined geometry. This route consisted of transferring the Cu_3BHT layer on substrates of SiO_2/Si with pre-patterned electrical contacts made of Ti/Au (as described above). In this case, all devices showed Ohmic responses which were reproducible over the whole sample area (8×8 mm^2). For that reason, this method was used to fabricate the devices studied and characterized in this work.

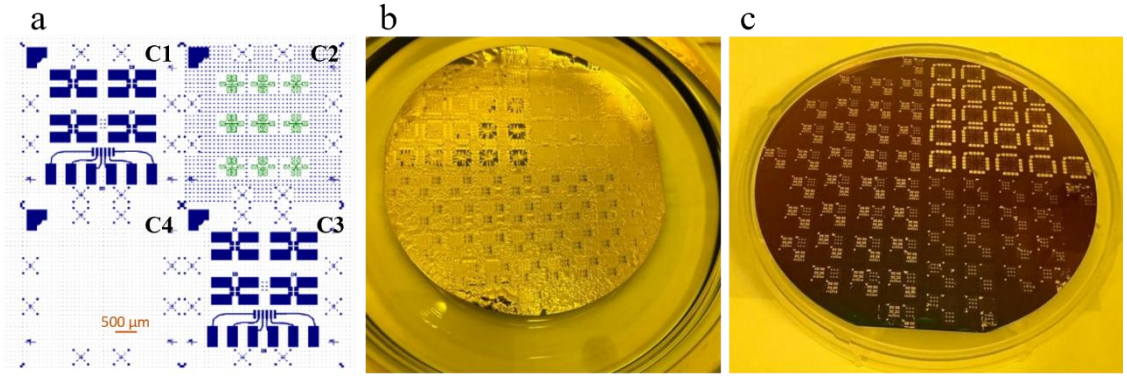

Figure S6. **a.** Design of metallic electrode motifs. Top left and bottom right: Van der Pauw and TLM configuration. Top right: hall bridges. Bottom left: blank. **b.** Four inches wafer after Ti/Au evaporation. **c.** Four inches wafer after lift-off.

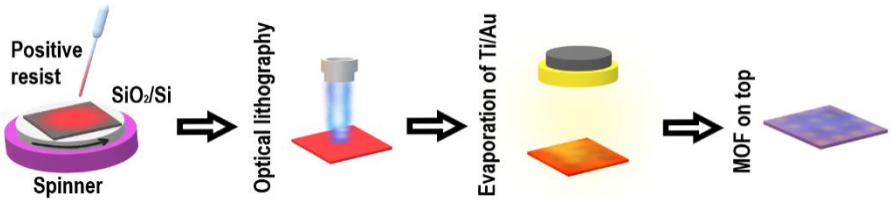

Figure S7. Scheme of Route 2 used to fabricate the Cu_3BHT devices characterized in this work.

After obtaining the sample, we secure it to the sample holder using double-sided copper tape, and we utilize gold wires to establish precise interconnections between the gold (Au) pads on the samples and the sample holder at room temperature and atmospheric pressure. This meticulous procedure involves employing gold wires with a thread height of 3 mm to ensure there is no unintended contact with the edges of the sample to prevent the current from inadvertently flowing across the Si substrate as illustrated in Figure S8.

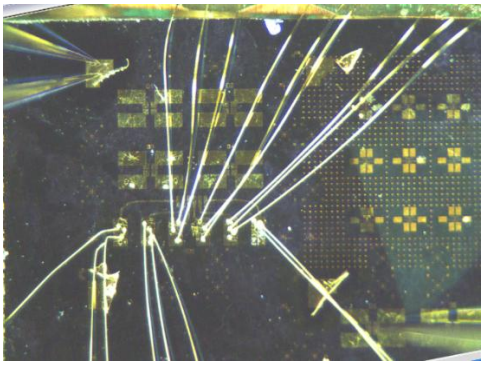

Figure S8. Gold wires connecting the sample to the sample-holder.

Using more than one wire per contact is advantageous for two reasons: it preserves electrical connection even if one of the wires disconnects and it enhances the heat dissipation through Joule effect.

To improve the attachment of the Au wires to the metal paths, we manually removed the Cu_3BHT on top of the motifs with a wooden tip before bonding the wire.

All experiments presented in this contribution were done with a DC current.

- ## Gate: Leakage checking

In our sample, a back-gate was incorporated to study the leakage current through the SiO_2. This was accomplished by connecting one probe to the gate contact and two probes to two electrodes of a selected device (see Figure S9.a). In this way, by applying a voltage across the SiO_2 (gate voltage, V_g) and a voltage between the device electrodes (sour-drain voltage, V_{SD}), we could measure the current flowing between the sample and the silicon substrate (leakage or gate current) and the current through the Cu_3BHT sample (source current).

First, no gate voltage was applied ($V_g = 0\,V$), obtaining a current through the Cu_3BHT layer of maximum 1 μA (contact separation of 50 μm) and a leakage current of less than 0.06 nA (see figure S9.b), implying that most of the current was flowing through the Cu_3BHT, and there was no significant leakage through the SiO_2.

The next measurement was made by applying a gate voltage ($V_g = 10\,V$). In this instance, the maximum leakage current was around 0.44 μA, comparable to the current through the Cu_3BHT layer (see figure S9.c). This suggested a significant leak through the substrate, and therefore this could affect the measurement of the Cu3BHT resistance accurately. To address this issue, we removed rests of Cu_3BHT material around the gate electrode using a wooden tip. As a result, the leakage current was reduced to nA, and once again, there was no observable leakage (see figure S9.d).

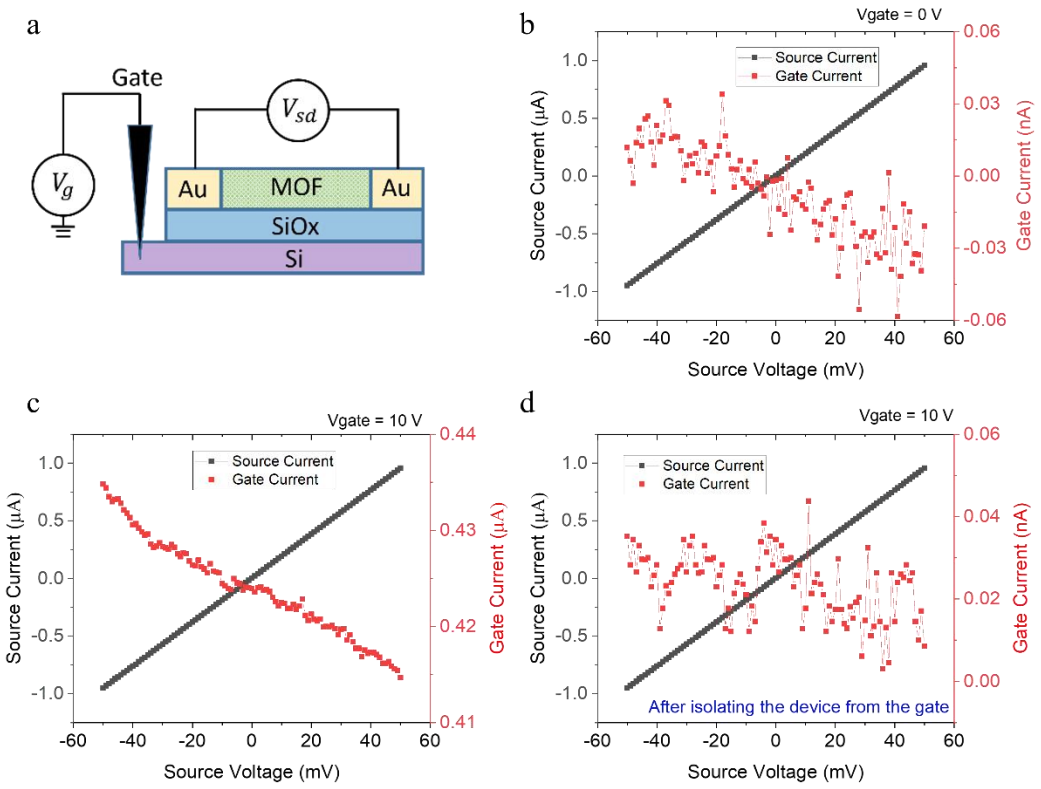

Figure S9. **a.** Schematics of the sample indicating the source-drain and gate contacts. Source Current (black squares) and Gate current (red squares) vs Source Voltage b. with no gate voltage applied., **c.** with V_G = 10 V and with **d.** V_G = 10 V after scratching around the gate contact.

For that reason, it is necessary to scratch the surface of Cu_3BHT around the gate.

- **Homogeneity and I-V measurement in different areas**

Our sample has a series of devices along its 8 × 8 mm^2, which we have used to check for homogeneity.

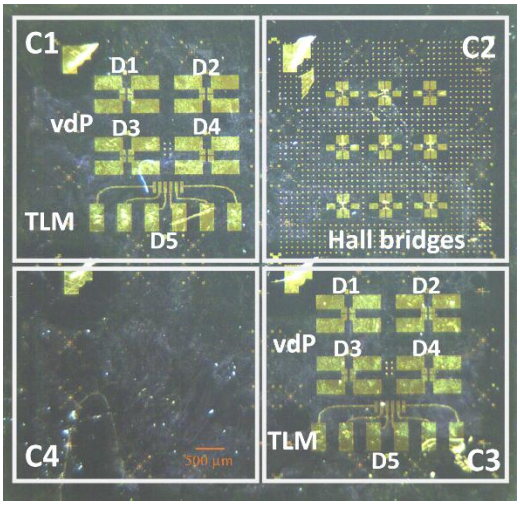

Figure S10. Optical image of monolayer Cu_3BHT on top of different device configurations.

In order to check the homogeneity in the electrical properties of the monolayer Cu_3BHT, we measured I-V characteristics in the 8 Van der Pauw devices in areas C1 and C3, see figure S10.

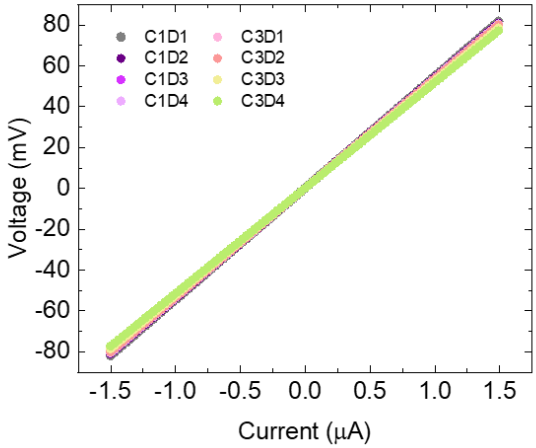

Figure S11. I-V characteristics of monolayer Cu_3BHT in different devices with contact separation of 50 μm, exhibiting ohmic responses with a relative dispersion in resistance values of 6%.

All the IV curves were ohmic, see Fig. S11. by By using Ohm´s law R=V/I, we determined the different resistances along the sample for a separation of 50 μm between probes:

$R_{C1\,D1} = 54.70\ k\Omega$; $R_{C1\,D2} = 54.15\ k\Omega$; $R_{C1\,D3} = 52.71\ k\Omega$; $R_{C1\,D4} = 53.84\ k\Omega$;

$R_{C3\,D1} = 53.12\ k\Omega$; $R_{C3\,D2} = 53.60\ k\Omega$; $R_{C3\,D3} = 52.53\ k\Omega$; $R_{C3\,D4} = 51.65\ k\Omega$;

The dispersion in resistance values is within 6%, indicating good homogeneity of our sample.

- ## Instruments

- He cryostat:

To measure the temperature dependence of resistance, we utilized an Optistat AC-V12 cryostat, capable of cooling down to 4.2 K. This is a closed-cycle helium cryostat that cools the sample space through helium gas expansion and compression cycles. To prevent air freezing and component obstruction, it includes a vacuum pump to reduce the internal pressure to around 10^{-5} mbar (10^3 Pa, 10^{-2} atm). Helium circulates in a closed loop: exiting the cryostat, it passes through a compressor that lowers He´s temperature and propels it back into the cryostat. The compressor is cooled by an external water circuit. This ensures that the helium is maintained at a temperature of 4 K. Thanks to this, the sample can be cooled while controlling its temperature was controlled by means of an Oxford 350 temperature controller.

The cryostat features a sample space with various pins for attaching the sample holder pins. Connection of the cryostat pins to the current source and voltmeter is achieved through a LEMO connector located on the cryostat's exterior.

- Keithley 2450:

It is a compact instrument, known as an SMU (Source Meter Unit), that allows for the application of current and measurement of voltage (or vice versa). The nominal output voltage ranges from ±20 mV (for measurements < 1 A) to ±200 V (for measurements < 100 mA), and the nominal output current is ±1 A (<20 V) and ±100 mA (<200 V).

- Probe station

The Everbeing manual probe station is configured to precisely measure 4-point current-voltage characteristics. It consists of four probes that can be position on the sample by using four micromanipulators. The sample is kept fixed to the chuck by vacuum. The probes are connected triaxial cables to a Keithley 4200-SCS Parameter Analyzer allowing measurements of sub pA currents. Probes are manually positioned, and a video camera with a microscope is used to navigate along the sample.

- Wire bonder

A wire bonder HB10 was employed to establish interconnections between the Au pads on the samples and the sample holder using Au wires. It is a semi-automatic wire bonder with a single bonding head that can operate in ball/wedge or wedge/wedge bonding mode. The Z axis is automatic/motorized. It has a touch screen that allows adjustment of parameters:

- Loop height (3 mm to avoid contact with the edge of the sample)
- Ultra sonic (U/S) energy (500 for the sample holder and 850 for the sample)
- Time (800 ms for the sample holder and 300 ms for the sample)
- Force (400 mN for the sample holder and 200 ms for the sample)

The settings can be adjusted from 0 to 2000 displaying the relative strength of the U/S signal to the tool. If the U/S is set with very low values, the strength of the U/S may not be enough to perform a bond, or it will perform a very weak bond.

It can bond wires with sizes from 17 μm to 75 μm.

- **Two- and four-probe T dependent resistance measurements**

As we discussed in the main text, the contact resistance in our devices is of the order of the Cu_3BHT resistance. We analyzed the difference between 2 and 4-probe method as a function of temperature, and we obtained the results shown in Fig. S12. When working with the 2-probe method, in addition to measuring the resistance of the sample, we also measure the contact resistance with the wires; since both resistances are comparable, we cannot determine the actual resistance value of the Cu_3BHT. For this reason, we need to use the 4-probe method. This difference in resistances becomes more pronounced as the temperature decreases, as we can see in Figure S12.a.

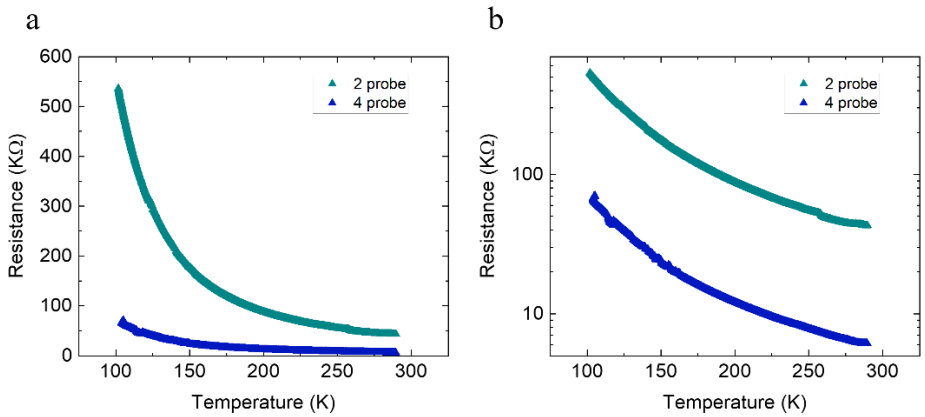

Figure S12. Electrical resistance of monolayer Cu_3BHT as a function of T measured by the 2- and 4- probe methods in **a.** linear scale and **b.** logarithmic scale.

The 2-probe resistance increased significantly when lowering the temperature as compared with the temperature evolution of the 4-probe resistance (see Figure S12.a). However, when we plot these results in logarithmic scale, the T dependent trend seems to be the same in both cases. This is more evident when we normalized both resistance curves by the values al T = 100 K as shows in Figure S13, suggesting that while contact resistance has an effect on the quantitative estimates, it does not have a strong impact over the T dependence.

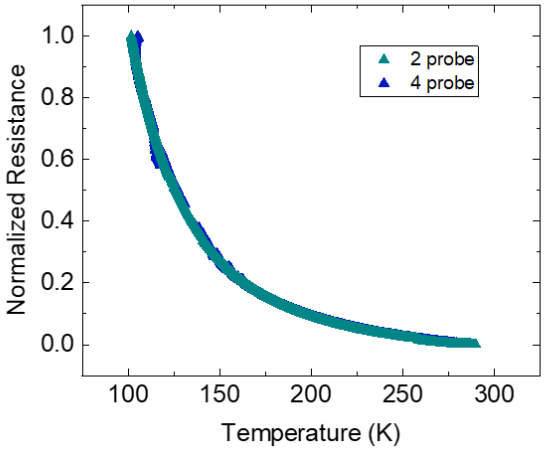

Figure S13. Electrical resistance of monolayer Cu_3BHT, measured by the 2- and 4-probe methods and normalized by R at 100 K, as a function of T.

- **Temperature dependence of resistivity**

The resistance vs temperature curves were measured using the 4-probe configuration in the TLM devices using the two most outer electrodes for applying current and measuring the voltage between the two inner electrodes. To obtain a magnitude that is independent of the sample's geometry, we calculated the resistivity as: $\rho = \frac{A}{d} R$, where A is the cross section of the device and d is the separation between voltage electrodes.

In successive measurements, we observe hysteresis (see Figure S14.a) where the resistivity undergoes a drastic change at low temperatures. This hysteresis is more pronounced at lower temperatures, but when zooming in at higher temperatures (200 K to 300 K), after a couple of cycles, it remains relatively constant. Additionally, Figure S14.b shows a significant jump in resistance at room temperature, which becomes five times greater after 8 loops.

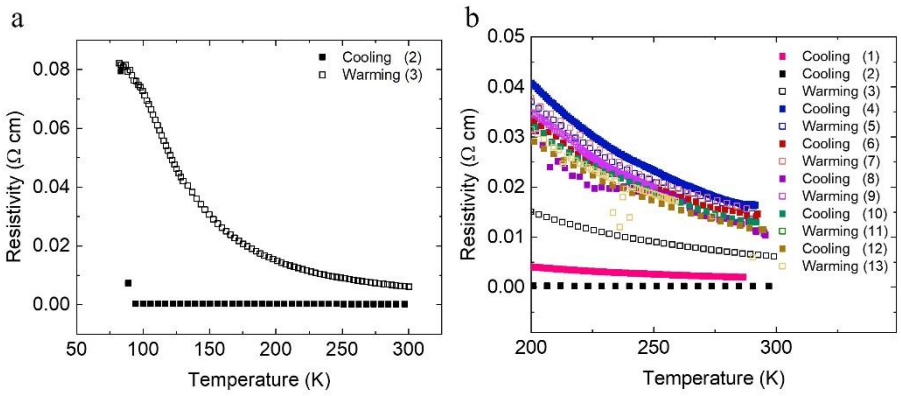

Figure S14. **a.** Resistivity-temperature dependence of monolayer Cu_3BHT showing a hysteresis at the first temperature cycle. **b.** Resistivity-temperature dependence of monolayer Cu_3BHT in different temperature cycles, where the numbers in parentheses indicate the order in which the measurement was conducted and the zoom from 200 K to 300 K.

After stabilization, we obtained a highly accurate linear fit log(σ) vs T in the temperature range from 300 K to 125 K as discussed in the main text. At 50 K, the sample undergoes a reproducible jump to another quasi-linear region, as illustrated in Figure S15.c where the whole temperature range measured is shown.

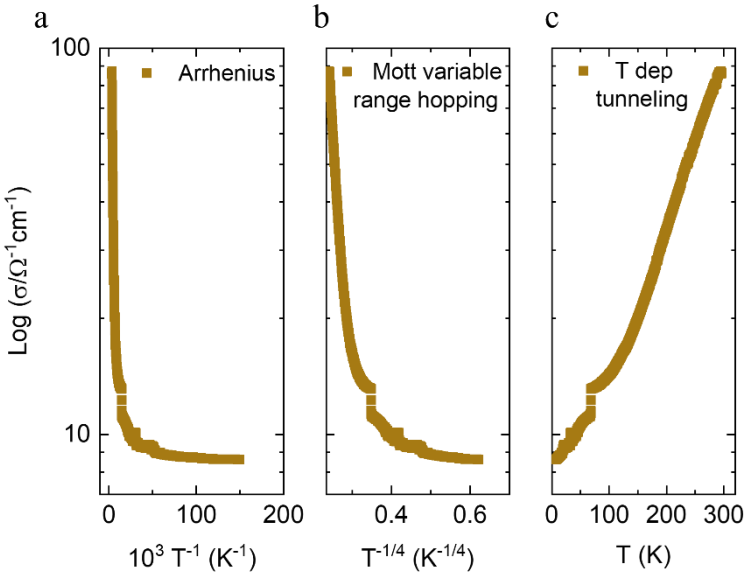

Figure S15. Log of conductivity vs **a.** 1/T (Arrhenius), **b.** $1/T^{1/4}$ (3D Mott variable-range hopping) and **c.** T (tunnelling). From 300 K to 4 K.

- ## VB-XPS characterization

The valence band measurements have been performed by XPS (X ray Photoelectron Spectroscopy) in a UHV (Ultra High Vacuum) chamber with a base pressure of 4×10^{-10} mbar. The XPS characterization has been done using a monochromatic Al-k_α as excitation source (1486.7 eV), a hemispherical electron analyzer (SPHERA U7) and a flood gun (Specs FG-500) to compensate the built-up charge (3eV, 40 μA). The binding energy correction for all the XPS measurements was taking the SiO_2 2p core level of the substrate centered at 103.6 eV as a binding energy reference (the native oxide of a Si crystal, normally centered at 99.4 eV) and the pass energy was fixed at 20 eV to have a resolution of 0.6 eV.

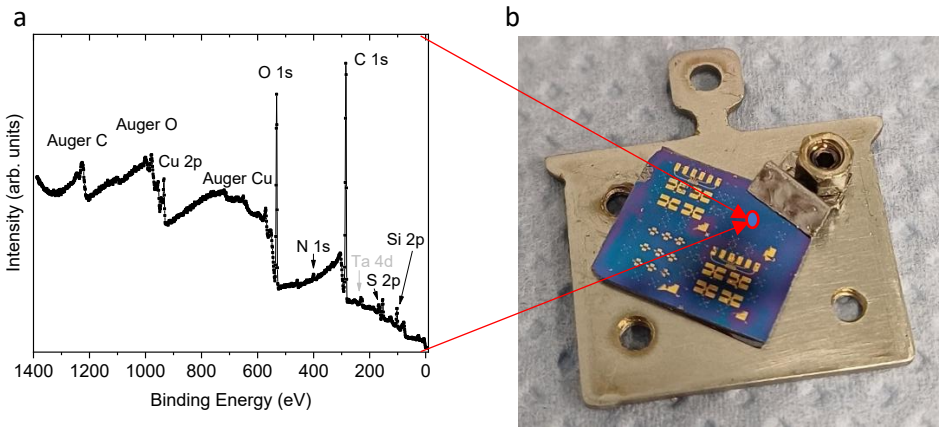

Figure S16: a. XPS Survey spectrum of Cu_3BHT sample measured in the red area marque on figure b. The small Ta peak detected belong to the Ta spring thar holds the substrate.

On the survey spectrum we observe all the elements present on the sample: C, O, Cu, S, N, Si and Ta.

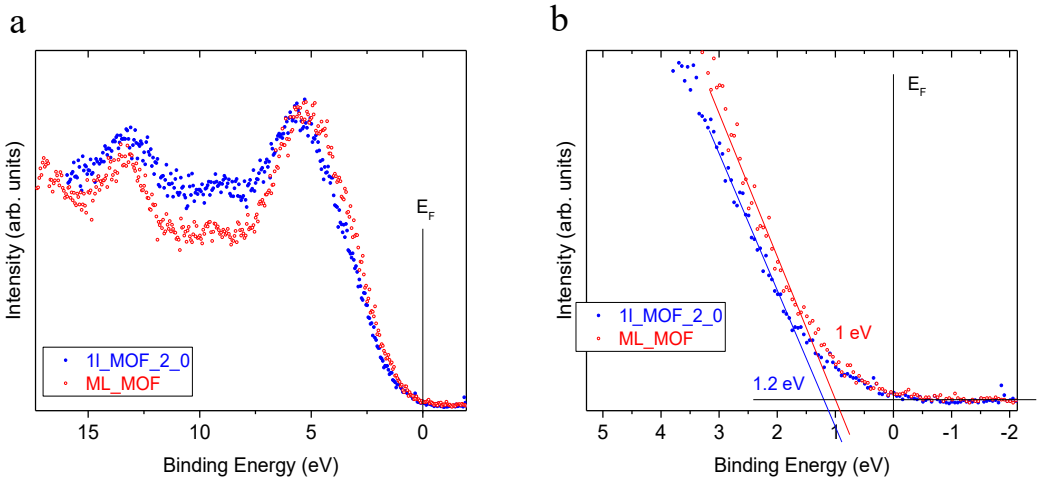

Figure S17. **a.** Valence band measured with XPS of Cu_3BHT. **b.** Zoom-in of the border of the band where an extrapolation of the spectrum should indicate the distance from the border of the valence band to the Fermi level.

- **Cu_3BHT monolayer structure with adsorber water**

To model the water adsorption on the Cu_3BHT structure, we have considered adsorption of single water molecule above a copper atom of the standalone wavy Cu_3BHT, to ascertain the adsorption

energy of 47 k J/mol, and mainly the full coverage of the coper atoms in the monolayer resulting in 6 adsorbed water molecules per Cu_3BHT structural unit (three H_2O from top, three H_2O from bottom). The average adsorption energy for one water molecule is 72 kJ/mol.

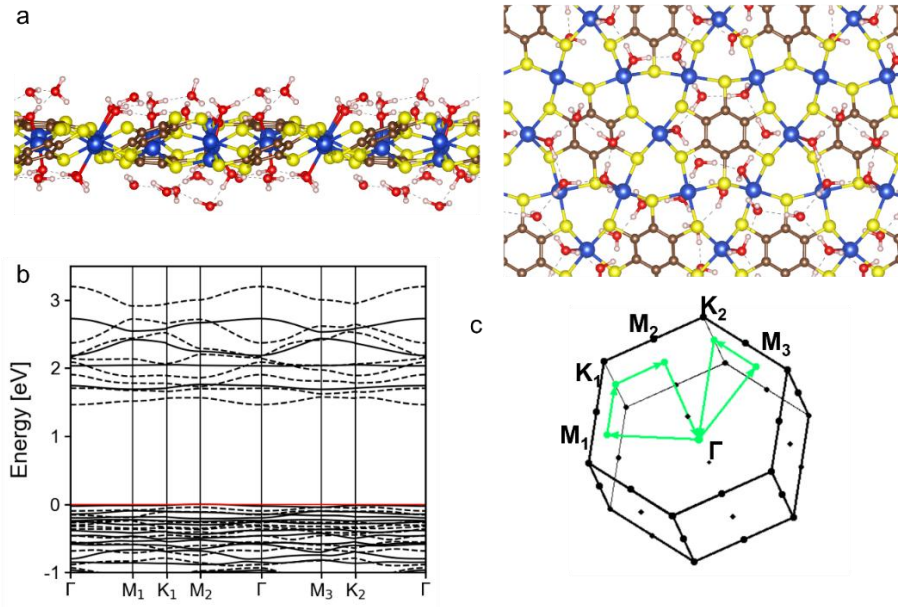

Figure S18. **a.** (100) side view and (001) top view of Cu_3BHT monolayer with 6 adsorbed water molecules per Cu_3BHT structural unit. The waviness has periodicity of 2×2 Cu_3BHT unit cells. **b.** Band structure of the wavy Cu_3BHT monolayer with 6 adsorbed water molecules per Cu_3BHT structural unit. **c.** High-symmetry k-points and path in the Brillouin zone.